This article has been accepted for publication in a future issue of this journal, but has not been fully edited. Content may change prior to final publication. Citation information: DOI 10.1109/TNSRE.2016.2536278, IEEE Transactions on Neural Systems and Rehabilitation Engineering

Gait Event Detection in Real-World Environment for Long-Term Applications: Incorporating Domain Knowledge into Time-Frequency Analysis

Siddhartha Khandelwal and Nicholas Wickström

***Abstract*—Detecting gait events is the key to many gait analysis applications that would benefit from continuous monitoring or long-term analysis. Most gait event detection algorithms using wearable sensors that offer a potential for use in daily living have been developed from data collected in controlled indoor experiments. However, for real-word applications, it is essential that the analysis is carried out in humans' natural environment; that involves different gait speeds, changing walking terrains, varying surface inclinations and regular turns among other factors. Existing domain knowledge in the form of principles or underlying fundamental gait relationships can be utilized to drive and support the data analysis in order to develop robust algorithms that can tackle real-world challenges in gait analysis. This paper presents a novel approach that exhibits how domain knowledge about human gait can be incorporated into time-frequency analysis to detect gait events from long-term accelerometer signals. The accuracy and robustness of the proposed algorithm are validated by experiments done in indoor and outdoor environments with approximately 93,600 gait events in total. The proposed algorithm exhibits consistently high performance scores across all datasets in both, indoor and outdoor environments.**

***Index Terms*—inertial sensors, accelerometer, wavelet transform, morlet, gait analysis, stride parameters, principles of gait**

I. Introduction

NORMAL gait consists of three primary components: locomotion, balance and ability to adapt to the environment [1]. This requires a balance between various interacting neuronal and musculoskeletal systems. Dysfunction in one or more of these systems can disturb gait, which elucidates the importance of gait analysis. In the temporal domain, the two most relevant events in a normal gait cycle are heel strike (HS) and toe off (TO); other parameters such as swing, stance and stride duration can be computed from them. Thus, identifying these events is the key to many gait analysis applications [2]–[9] that would benefit from long-term, continuous monitoring in humans' natural environment, enabling gait assessment and interventions that have not previously been possible [10]. The present state of practice is to perform clinical gait analysis in controlled gait labs equipped with stationary sensor systems such as motion capture systems and force plates [11]. Although these systems provide rich and accurate information, they are inadequate for use in daily life as they are immobile, expensive, require high operational competence and provide information that is restricted to only a couple of steps. Foot switches such as force sensitive resistors (FSRs) provide contact timing information and are often used as the reference method in determining the accuracy of gait event detection in other systems [2], [12]–[14]. However, they do not provide any kinematic data or spatial information during swing phase, which are important aspects in pathological gait assessment [15]. Alternatively, inertial sensors such as accelerometers and gyroscopes can be used for gait assessment as they provide spatio-temporal information and can be used in combination to estimate parameters such as the trajectory of foot during gait [16]. Technological advancements have made them miniature, low-powered, durable, inexpensive and highly mobile, thus making it possible to collect long-term data from daily life. While some researchers have developed gait event detection algorithms from gyroscope data, others have developed from accelerometer signals [17]. In either of these situations, researchers could potentially benefit by applying improved algorithms to existing gait databases and utilizing them for future applications and further gait analysis. In the context of gyro-based algorithms, many methods have been developed from angular velocity signals obtained from shank-attached gyroscopes. For example, the approach in [18] uses adaptive thresholds while [13], [19] use peak detection to identify HS and TO from angular velocity signals. Other approaches include [20], where the gait cycle is divided into four gait phases represented in the form of a state machine and the transitions are governed by a knowledge-based algorithm, and [21], where an online Hidden Markov Model based method is presented. In [12], a wavelet based method is used to search for peaks associated with HS and TO which is modified in [22], such that the method can be used with minimal time delay. On the other hand, accelerometers are also being increasingly used as they are low powered devices, in the range of few microamperes, and have been shown to provide reliable measures of gait parameters [17], [23]. Most algorithms analyze signals obtained from individual accelerometer axis by positioning the sensor in a specific pre-defined orientation [2], [3], [13], [24]–[28] with the assumption that the accelerometer shall stay statically positioned throughout the experiment. However, it is quite likely that external factors might disturb the original configuration during long-term analysis [28], and thus either the axis alignment should be checked and readjusted frequently or the exact orientation of the accelerometer must be known throughout, to

The authors are with the School of Information Technology, Halmstad University, 301 18 Halmstad, Sweden (e-mail: siddhartha.khandelwal@hh.se, nicholas.wickstrom@hh.se).

This article has been accepted for publication in a future issue of this journal, but has not been fully edited. Content may change prior to final publication. Citation information: DOI 10.1109/TNSRE.2016.2536278, IEEE Transactions on Neural Systems and Rehabilitation Engineering

compensate for the misalignment of the axes. An alternative is to analyze the magnitude of the resultant accelerometer signal instead which makes it invariant to individual axis alignment, as done in [4], [29]. While some methodologies instruct subjects to walk in a straight line or a given path at a self-selected pace [4], [13], [27], [29], others either pre-define a set of walking speeds or ask the subjects to walk slowly, normal and fast, in order to test the algorithmic robustness to different velocities [3], [14], [24]–[26], [28]. A number of algorithms apply thresholds either to filtered accelerometer signals or use them at some intermediate stage after signal transformation, to perform peak detection for identifying events [25], [28], [29]. The performance of such algorithms is usually dependent on choosing the optimum values of these thresholds and tuning other parameters associated with them. Another approach is the use of machine learning techniques that depend strongly on labelled training data [2], [27]. Since they are data-driven approaches that resemble a black-box model [26], not only might they be difficult to interpret by clinicians [30] but it also remains unclear whether and how often such a system would need to be retrained with changing scenarios. Other approaches include [4], where a rule-based state machine is realized with four gait states, namely, mid-stance, pre-swing, swing and loading response; and the state transitions are determined by five reference signals derived from tri-axial accelerometer signals. In recent years, wavelet transforms are being increasingly used for gait analysis [31] and in particular to detect gait events [12], [27], [32]–[35]. In [27], wavelet transform is used to express the raw acceleration signals in time-frequency space which gives high dimensionality features. Then dimensionality reduction is done using a manifold embedding algorithm to project the data to a smaller dimensional subspace in order to obtain a minimal subset of features that contain salient signal information. Finally, a Gaussian mixture model (GMM) is applied to classify each time sample as HS, TO or no-event.

The existing gait event detection algorithms that offer potential for use in daily living have been developed from data collected in controlled indoor experiments placing a number of assumptions on the experimental design itself. On the other hand, human gait in the real-world is quite dynamic, and frequently involves different gait speeds, changing walking terrains, varying surface inclinations and regular turns among other things. Although some recent attempts have been made [27], it is highly challenging to imitate these scenarios in labs or corridors. However, portable wearable systems can be used to carry out long-term experiments directly in natural human environments. Moreover, it is essential to distinguish between walking and non-walking tasks prior to applying the event detection algorithms [36] unless such a feature is included in the algorithm itself. Instead of relying only on data-driven approaches, existing domain knowledge about the fundamental principles of gait and other prior auxiliary information could be used to help guide the data analysis in order to achieve greater robustness and accuracy. This paper proposes a novel approach that exhibits how domain knowledge about human gait can be incorporated into time-frequency analysis in order to detect gait events from walking and running segments of long-term accelerometer signals. The performance of the proposed method is validated by experiments done in indoor and outdoor environments, and the results are compared with two state of the art algorithms. The rest of this paper is organized as follows. Section II describes the proposed approach and Section III outlines the data collection procedure. Section IV presents the results of applying the algorithm in indoor and outdoor environments. Finally, Section V discusses and concludes this paper. The Appendix provides relevant details required to implement a part of the proposed algorithm.

II. Proposed Algorithm

A. Domain Knowledge

To detect gait events from long-term accelerometer signals, the algorithm should be able to tackle real-world issues such as different gait speeds, changing environments and disturbances in sensor orientation. To achieve this goal, domain knowledge in the form of principles or underlying fundamental gait relationships between various governing gait parameters can be utilized to drive and support the analysis. One such underlying gait principle is the frequency relationship that is present between gait event and gait cycle, i.e. the frequency of the event (HS and TO) is twice that of the cycle. In the proposed algorithm, the use of this knowledge is two-fold. The first is to logically reason around choosing the appropriate mother wavelet for wavelet transform, as there are insufficient guidelines on the selection of wavelet basis function for gait signals [31]. The second involves incorporating this fundamental frequency relationship into the signal analysis procedure, which allows the algorithm to effectively tackle changes in gait speeds. Thus, the raw acceleration signal is first pre-processed, and this is followed by time-frequency analysis guided by domain knowledge.

B. Time-Frequency Analysis

As mentioned in Section I, it is quite likely that the original sensor orientation may be disturbed during long-term analysis. Hence, to avoid misalignment issues, the magnitude of the resultant accelerometer signal, Acc_r, henceforth referred to as the 'composite acceleration signal', is computed as:

$$Acc_r = \sqrt{{acc_x}^2 + {acc_y}^2 + {acc_z}^2} \tag{1}$$

where acc_x, acc_y, acc_z are the signals obtained from each individual axis of the 3-axes accelerometer, respectively. Fig. 1a shows the HS and TO events present in one gait cycle of the composite acceleration signal. To exemplify the time-frequency relationship between gait event and gait cycle, continuous wavelet transform (CWT) is used [37]. It produces a time-frequency decomposition where both, short-duration high frequency and long-duration low frequency information can be captured simultaneously. Another key advantage of wavelet techniques is the variety of wavelet basis functions available for signal analysis [38]. Domain knowledge is used to select the appropriate wavelet based on the following criteria:

- It should highly correlate with both, the frequency of the events and the frequency of the cycle in Acc_r, in order to clearly distinguish these spectral components in time.

This article has been accepted for publication in a future issue of this journal, but has not been fully edited. Content may change prior to final publication. Citation information: DOI 10.1109/TNSRE.2016.2536278, IEEE Transactions on Neural Systems and Rehabilitation Engineering

- It should be symmetric to avoid spectral domain skewness. Moreover, a wavelet with a high degree of symmetry leads to good performance for the analysis of periodic signals [39].

Thus, the Morlet wavelet is chosen, which is a complex sinusoid modulated by a Gaussian. It is defined as $\psi_0(\eta) = \pi^{-1/4}\, e^{i\omega_0\eta}\, e^{-\eta^2/2}$ where ω_0 is the frequency and η is a nondimensional time parameter [40]. The CWT of a discrete time signal, x_n, with equal time spacing δ_t, is defined as the convolution of x_n with a scaled and translated mother wavelet $\psi_0(\eta)$:

$$W_n(s) = \sum_{n'=0}^{N-1} x_{n'}\ \psi^* \left[\frac{(n'-n)\delta_t}{s} \right] \tag{2}$$

where the $(*)$ indicates the complex conjugate, s is the wavelet scaling factor and n is the localized time index. Fig. 1b shows the CWT of the Acc_r signal where the time-frequency relationship between the individual gait events of HS and TO and their corresponding gait cycle can be simultaneously observed. The event coefficients exist towards the finer scales that correspond to higher frequencies while the cycle coefficients exist towards the coarser scales corresponding to lower frequencies. As shown in Fig. 1c, the event regions can be located by defining appropriate boundaries along the spectral and temporal axes and the position of the event can be derived by fitting a 2-D Gaussian distribution over this region. However, defining these boundaries is a challenging task as changes in gait speed cause the event and cycle coefficients to shift along the scales, as shown in Fig. 1d, because of shifts in the local signal energy. Faster gait speeds mean higher gait frequency, and thus the event and cycle coefficients exist towards the finer scales and vice-versa. Hence, a tracking procedure is proposed that utilizes domain knowledge to detect these transitions along the scales such that the event regions can be determined.

Thus, as depicted in Fig. 4, the proposed algorithm consists of three major steps that are performed systematically. These steps are elaborated in the following subsections.

1) Pre-processing: First, composite acceleration signal Acc_r is computed from the individual acceleration signals obtained from the 3-axes accelerometer using eq. 1. Then, the CWT of this signal is computed using eq. 2, by convoluting Acc_r with a scaled and translated real-valued Morlet wavelet to obtain $W_n(s)$. The range of scales to be considered for CWT can be estimated from the non-linear frequency-scale relationship of the Morlet [40], as shown in Fig. 2a.

2) Tracking the gait speed changes: As explained earlier, changes in gait speed cause transitions of the event and cycle coefficients along the scale or spectral axis and these transitions need to be detected in order to find appropriate event region boundaries. This is done by defining a tracking procedure that utilizes the domain knowledge about the frequency relationship between the gait event and cycle, i.e. the frequency of the event (HS and TO) is twice that of the cycle. The relative contribution of these two major frequencies to the total signal energy at a specific scale s can be measured by

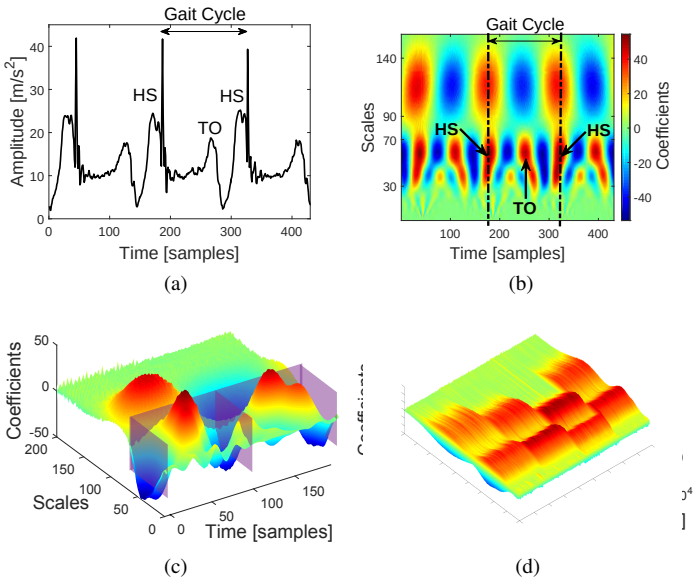

Fig. 1. (a) HS and TO events in one gait cycle of a composite acceleration signal, Acc_r, obtained from the 3-axis accelerometer attached to the right ankle. The amplitude of Acc_r is approx. 10 m/s^2 during stance due to the effect of the gravitational component. (b) Time-frequency representation (top view) of the composite acceleration signal using CWT by the Morlet wavelet. The HS and TO events exist in the finer scales (30-70) while the corresponding gait cycle exists along the coarser scales (90-140). The color bar presented in this subfigure is also applicable to subfigures 1c and 1d. (c) Example of spectral-temporal boundary, shown as semi-transparent walls, around the HS and TO region in one gait cycle. (d) Example of CWT coefficients shifting along the spectral axis with changes in gait speed. With faster gait speeds, the event and cycle coefficients shift towards the finer scales and vice-versa.

the scale-dependent energy density spectrum E_s, as:

$$E_s = \sum_{n=0}^{N-1} |W_n(s)|^2, \qquad s \in [1, s_{\max}] \tag{3}$$

where $|W_n(s)|^2$ is the 2-D wavelet energy density function known as the scalogram that measures the total energy distribution of the signal [37]. Peaks in E_s highlight the dominant energetic scales and it is the event and cycle peaks that contribute to most of the signal energy in the spectral domain. Thus, the energy density spectrum E_s, of the CWT coefficients can be approximated as a mixture of two 1-D Gaussian distributions, where each Gaussian represents the spectral signal energy of the event and cycle, respectively as:

$$E_s \approx \underbrace{a_e\, e^{-\left(\frac{s-\mu_e}{\sigma_e}\right)^2}}_{event} + \underbrace{a_c\, e^{-\left(\frac{s-\mu_c}{\sigma_c}\right)^2}}_{cycle} \tag{4}$$

In addition, the event-cycle frequency relationship can be used to associate the two Gaussian means in E_s as:

$$\mu_c = 2\,\mu_e \tag{5}$$

where μ_e and μ_c are the two most dominant scales representing event and cycle energy, respectively. Using this approximation, an *a priori* energy density spectrum estimate E_s^- is formulated which is used to start the tracking procedure. The value of Gaussian mean μ_e^- (in scale units) can be obtained from the frequency-scale relationship of the Morlet, shown in Fig. 2a, by making an initial assumption of the frequency

This article has been accepted for publication in a future issue of this journal, but has not been fully edited. Content may change prior to final publication. Citation information: DOI 10.1109/TNSRE.2016.2536278, IEEE Transactions on Neural Systems and Rehabilitation Engineering

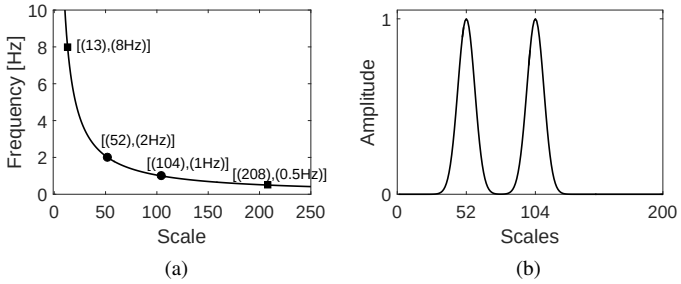

(a) (b)

Fig. 2. (a) Frequency-scale relationship for Morlet wavelet. So, for example, if the minimum gait frequency is assumed to be 0.5Hz, then the corresponding maximum scale to be considered for analysis is 208, denoted $s_{\max}$. (b) *A priori* energy density spectrum estimate E_s^- formulated by assuming the initial frequency of the event to be 2Hz, i.e. $\mu_e^- = 52$ and $\sigma^- = 9$.

of the event. The corresponding μ_c^- is then computed using eq. 5. Also for simplicity, both Gaussians are assumed to be of unit amplitude and equal standard deviation σ^-, well representing event and cycle energies. With these simplified initial parameters, E_s^- can be formulated (shown in Fig. 2b) as:

$$E_s^- = e^{-\left(\frac{s-\mu_e^-}{\sigma^-}\right)^2} + e^{-\left(\frac{s-2\,\mu_e^-}{\sigma^-}\right)^2}, \quad s \in [1, s_{\max}] \qquad (6)$$

To track the transitions of event and cycle coefficients along the spectral axis, an overlapping running window is taken along the temporal axis of the CWT coefficients. Within each window, E_s is computed using eq. 3 and is cross-correlated with the *a priori* estimate E_s^-, which helps in extracting event and cycle spectral information from E_s using the Gaussian approximation formulation given in eq. 4. Based on the extracted information, the parameters in E_s^- are updated to form an *a posteriori* estimate $\hat{E}_s$, which serves as the prior for the next window. See the Appendix and Figures 6 and 7 for details of the entire tracking procedure within a window.

3) Locating and identifying the gait event: In order to set up appropriate boundaries to define spectral-temporal event regions as shown in Fig. 1c, the information stored in the tracking procedure is utilized. The Gaussian means $\hat{\mu}_{e,r}$ and $\hat{\mu}_{c,r}$ that are stored in every window r hold information about the local frequency of the event and cycle for the time duration of that window. By successively compiling them from all windows and selecting the CWT coefficients at those particular scales, two distinct temporal signals are obtained that match the frequency of the event and cycle in the composite acceleration signal as shown in Fig. 3. The discrete time signal matching the frequency of the event, denoted x_n^e, is obtained as:

$$x_n^e \triangleq W_n[(\hat{\mu}_{e,0}, \hat{\mu}_{e,1}, ..., \hat{\mu}_{e,r}, ..., \hat{\mu}_{e,\frac{N}{M}-1})^T] \qquad (7)$$

where W_n is the CWT coefficients computed using eq. 2, r is the window index, M is the window step, n is the discrete time sample and N is the total number of samples in the composite acceleration signal. Similarly, the discrete time signal matching the frequency of the cycle, denoted x_n^c, is obtained as:

$$x_n^c \triangleq W_n[(\hat{\mu}_{c,0}, \hat{\mu}_{c,1}, ..., \hat{\mu}_{c,r}, ..., \hat{\mu}_{c,\frac{N}{M}-1})^T] \qquad (8)$$

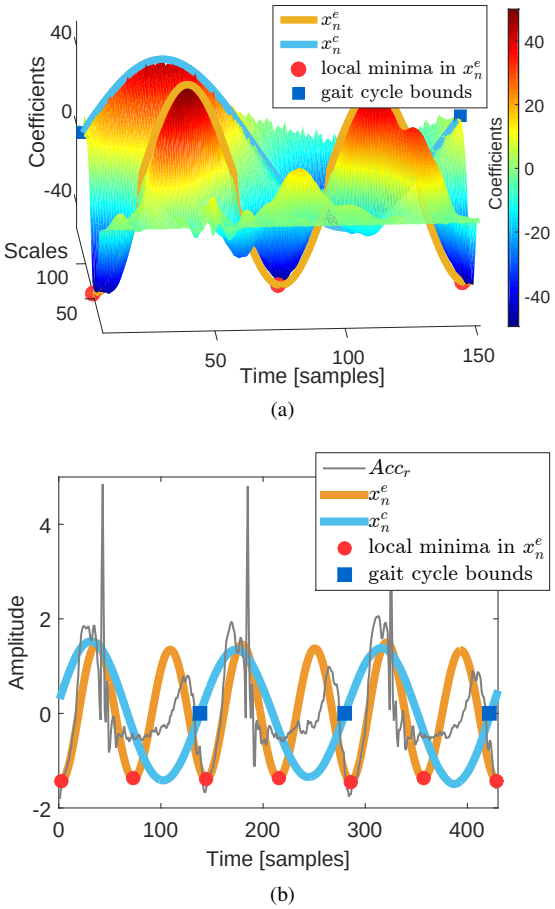

(a) (b)

Fig. 3. (a) The figure shows CWT coefficients from one gait cycle. The two temporal signals, x_n^e and x_n^c, are obtained by selecting the CWT coefficients from scales corresponding to Gaussian means $\hat{\mu}_{e,r}$ and $\hat{\mu}_{c,r}$ that are stored in every window r. As shown, x_n^e and x_n^c hold information about the local frequency of the event and cycle. The local minima points (m_i) in x_n^e give the temporal bounds for individual event regions. The positions where the signal x_n^c changes sign from negative to positive mark the beginning and end of consecutive gait cycles. (b) Example of the two temporal signals, x_n^e and x_n^c, obtained after low-pass filtering, that match the frequency of the event and cycle in the composite acceleration signal, Acc_r, respectively. All signals have been standardized using zscore to scale them into the figure.

In order to remove high frequency noise and window edge effects, both signals, x_n^e and x_n^c, are low-pass filtered using a *zero-phase* FIR filter with a cut-off frequency that is higher than the maximum expected gait frequency, taken to be 8Hz. The local minima points in x_n^e, defined by the set $\{m\colon m$ is the local minimum in $x_n^e\}$, provides the bounds for the individual event regions along the temporal axis (shown as circular dots in Fig. 3). To determine the corresponding spectral boundary for the event region, the scale $s_{\lambda,r}$ which distinguishes the event and cycle spectral energies, is successively compiled from all windows as:

$$s_{\lambda,n}^e \triangleq [s_{\lambda,0}, s_{\lambda,1}, ..., s_{\lambda,r}, ..., s_{\lambda,\frac{N}{M}-1}]^T \qquad (9)$$

So for a given temporal bound $m_i(n)$, the corresponding spectral bound is given by the scale interval $[1, s_{\lambda,n}^e]$. Thus, a 2-D spectral-temporal event region $\mathfrak{R}(n,s)$ is located as:

$$\mathfrak{R}_i(n,s) = W_{n\in[m_i, m_i+1]}(s \in [1, s_{\lambda,n}^e]) \qquad (10)$$

This article has been accepted for publication in a future issue of this journal, but has not been fully edited. Content may change prior to final publication. Citation information: DOI 10.1109/TNSRE.2016.2536278, IEEE Transactions on Neural Systems and Rehabilitation Engineering

The temporal position of the maximum CWT coefficient value in $\mathfrak{R}_i(n,s)$ could be simply used to estimate the event. However, highly noisy signal segments in Acc_r could lead to multiple local maxima in those CWT event regions and higher uncertainty in the precise location of the event. Thus, a 2-D Gaussian distribution fitting is done over each such spectral-temporal event region $\mathfrak{R}_i(n,s)$, such that the peak of the 2-D Gaussian fit gives the estimated location of the gait event in scale and time. Time signal x_n^c is then used to identify an event as an HS or TO. The positions where the signal x_n^c changes sign from negative to positive gives the temporal bounds for consecutive gait cycles (shown as squares in Fig. 3). Thus, within every gait cycle, the first event is labelled as an HS and the next as a TO.

C. Performance Assessment

Two state of the art algorithms, Rueterbories et al. ($\mathcal{A}_R$) [4] and Aung et al. ($\mathcal{A}_A$) [27], introduced earlier in Section I, were also implemented in order to compare them with the proposed method ($\mathcal{A}_{PM}$). The method of Hanlon et al. [41] was adopted to compute the ground truth (GT) gait events from the FSR measurements. A threshold value representing 39% of the maximum FSR value was used to identify the HSs on the rising edge of the FSR signal. The same procedure was repeated to identify the TOs after excluding the HS segments (HS$\pm$10 samples) from the signal. The matching between the actual gait events from the GT and the events detected by the proposed algorithm was based on a temporal tolerance of $\pm$5 samples or $\pm$0.039s. Any event missed by the FSR but detected by the algorithms implemented was automatically considered a false positive since the FSR was considered to be the GT. Statistical measures of sensitivity, specificity and F1 score were computed [42]. Conventionally, Mean Absolute Error (MAE) is used to present the temporal accuracy of a method in detecting gait events. The MAE was calculated (in samples) as the mean of the absolute temporal difference between the true positives of the algorithm and the corresponding GT events. Any constant bias was removed prior to the MAE calculation, for all algorithms. However, few true positives could lead to a low MAE value, indicating high accuracy even though many false positives might be detected by the method. Thus, the stride time was calculated and the Kolmogorov-Smirnov (KS) test was used to test the null hypothesis that the stride time samples from the algorithm and the GT came from the same empirical distribution [43]. If they did not, then the test rejected the null hypothesis at the 5% significance level. The KS test result provided an alternate perspective on the accuracy of a method as it took the entire stride time distribution into account, i.e. including both true positives and false positives. The data collected were divided into training and test data as the methodology in $\mathcal{A}_A$ required training of the model parameters. One third of the total number of subjects from the indoor and outdoor experiments were randomly selected to represent the hold-out test data. The purpose of this was to test the algorithmic performance in subjects that were not included in the training procedure. Sensitivity, specificity and the MAE of all algorithms were computed from the hold-out test data. However, the F1 score was computed by including the data from all subjects. Welch's t-test was used to find any significant differences between the F1 scores of any two sample groups.

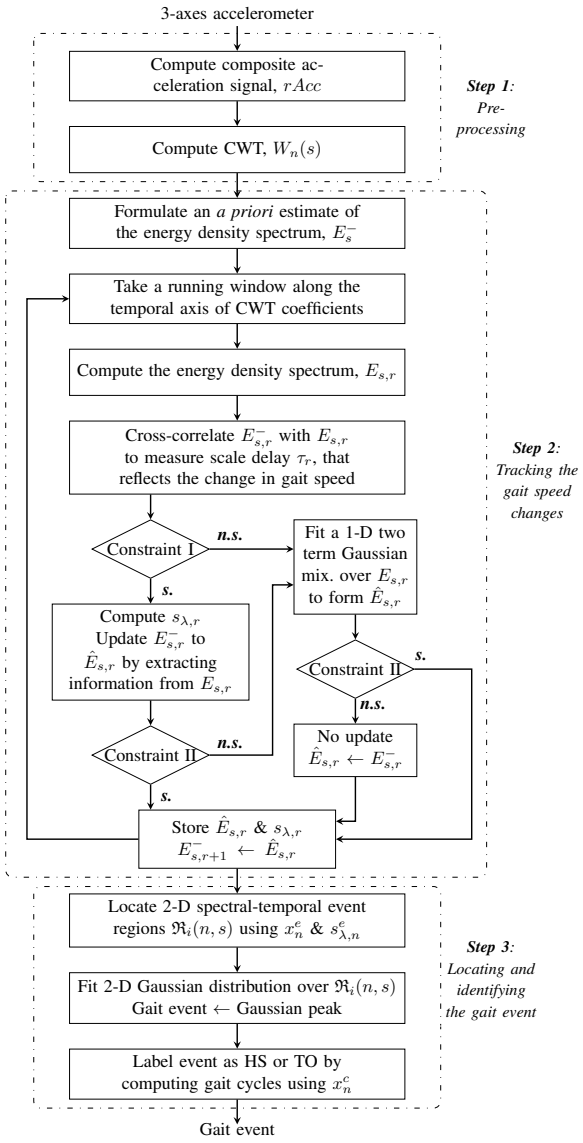

Fig. 4. Flow of the proposed gait event detection algorithm. The abbreviations 's.' and 'n.s.' stand for 'satisfied' and 'not satisfied', respectively. $E_{s,r}^-$, $E_{s,r}$ and $\hat{E}_{s,r}$ represent the *a priori*, current and *a posteriori* energy density spectrum estimates in the current window index r, respectively. $E_{s,r+1}^-$ represents the *a priori* estimate in the next window with index $r+1$.

III. Experiments

The study involved 20 healthy subjects (12 males and 8 females, average age: 33.4$\pm$7 years, average weight: 73.2$\pm$10.9 kg, average height: 172.6$\pm$9.5 cm) with 11 subjects participating in indoor and 9 participating in outdoor experiments. Each subject had a 3-axes Shimmer3 accelerometer ($\pm$ 8g) attached to both ankles using Velcro straps. For the left ankle, the accelerometer axis was positioned with the y-axis pointing downward and the x-axis to the anterior direction while, for the right ankle, the accelerometer was casually attached without

This article has been accepted for publication in a future issue of this journal, but has not been fully edited. Content may change prior to final publication. Citation information: DOI 10.1109/TNSRE.2016.2536278, IEEE Transactions on Neural Systems and Rehabilitation Engineering

TABLE I
SUMMARY OF THE EXPERIMENTS CARRIED OUT IN INDOOR AND OUTDOOR ENVIRONMENTS.

No. of subjects	Environment	Type of activity	Description	Speed	Approx. duration (minutes)	Total no. of gait events recorded
11	Indoor - Treadmill	Walk & run	Start walking and switch to running at any comfortable speed	4km/hr to 8km/hr; increasing in steps of 0.4km/hr every minute	10	30944
		Walk	Treadmill is set to (5°,0°,10°,0°,15°,0°) inclinations with 2 mins at each angle	Self-selected speed	12	25631
	Indoor - Flat space	Walk	Walking without any restrictions	Self-selected speed	3	7361
		Run	Steady running or jogging	Self-selected speed	3	10130
9	Outdoor - Street	Walk	Walking without any restrictions	Self-selected speed	3	10844
		Run	Steady running or jogging	Self-selected speed	3	8684*

* Two subjects did not complete the entire duration of the activity due to bad weather conditions.

any planned orientation. The subjects were provided shoes that had force sensitive resistors (FSRs) fixed at the extreme ends of the sole in order to provide the ground truth values for HS and TO. Both, the accelerometer and the FSRs had a sampling frequency of 128Hz, and the FSR output was stored locally on the Shimmer3 microSD card using an external expansion board. After every experiment, the data was transferred to a remote computer and the analysis was made offline using MATLAB v8.5 (MathWorks, USA). Informed consent was obtained from all subjects prior to the experiments. The study was approved by and all procedures were conducted in accordance with the guidelines of the Ethical Review Board of Lund, Sweden. Table I summarizes the experiments carried out in different environments. The indoor experiments were conducted on the treadmill and in a large, empty flat space. The outdoor experiments were conducted in the form of a closed path on a street that was approximately 50% flat and the rest being equally uphill and downhill. The path included four turns, and the uphill and downhill inclination angles ranged between 5° and 10°. Except when on the treadmill, the subjects were free to select their pace and change directions during all other activities. Manual inspection revealed that, for some data sets, few events were missed due to extremely low FSR values. The percentage of the missed FSR events for indoor and outdoor data sets was 0.05% and 0.09%, respectively. Four subjects from the indoor and three subjects from the outdoor experiments were selected at random to act as the hold-out test data.

TABLE II
MEAN (AND STANDARD DEVIATION) OF THE PERFORMANCE SCORES COMPUTED FOR INDOOR (FLAT SPACE) WALKING TEST DATA. $\mathcal{A}_{\mathrm{PM}}$, $\mathcal{A}_{\mathrm{A}}$ & $\mathcal{A}_{\mathrm{R}}$ STAND FOR PROPOSED METHOD, METHOD [27] AND METHOD [4].

Performance measures		Indoor walk: Flat space			
		LF		RF	
		HS	TO	HS	TO
Sensitivity	$\mathcal{A}_{\mathrm{PM}}$	**0.99** (0.00)	**0.98** (0.03)	**0.99** (0.00)	**0.99** (0.00)
	$\mathcal{A}_{\mathrm{A}}$	0.80 (0.36)	0.91 (0.10)	**0.99** (0.00)	0.97 (0.02)
	$\mathcal{A}_{\mathrm{R}}$	0.98 (0.00)	0.97 (0.03)	0.98 (0.00)	0.98 (0.01)
Specificity	$\mathcal{A}_{\mathrm{PM}}$	**0.99** (0.00)	**0.98** (0.03)	**0.99** (0.00)	**0.99** (0.00)
	$\mathcal{A}_{\mathrm{A}}$	0.96 (0.05)	0.00 (0.00)	0.95 (0.05)	0.07 (0.08)
	$\mathcal{A}_{\mathrm{R}}$	**0.99** (0.00)	0.97 (0.03)	**0.99** (0.00)	0.98 (0.01)
MAE (in samples)	$\mathcal{A}_{\mathrm{PM}}$	**0.55** (0.66)	**0.77** (0.94)	**0.66** (0.69)	**0.62** (0.73)
	$\mathcal{A}_{\mathrm{A}}$	0.85 (0.88)	0.90 (0.98)	0.74 (0.80)	0.88 (1.18)
	$\mathcal{A}_{\mathrm{R}}$	0.67 (0.74)	0.98 (0.98)	0.86 (0.85)	0.79 (0.77)
KS test ($\frac{\text{datasets not rejected}}{\text{total datasets tested}}$)	$\mathcal{A}_{\mathrm{PM}}$	**4/4**	**4/4**	**4/4**	**4/4**
	$\mathcal{A}_{\mathrm{A}}$	2/4	0/4	3/4	0/4
	$\mathcal{A}_{\mathrm{R}}$	**4/4**	**4/4**	**4/4**	**4/4**
No. of GT gait events		682	678	680	678

IV. RESULTS

Table II shows the mean and standard deviation of these performance scores for indoor (flat space) walking test data, which is the environment in which most gait event detection algorithms have been developed. Each cell in the table displays a distinct performance score for detecting HS or TO from the accelerometer signal obtained from the left (LF) or right foot (RF). The column under LF displays the score when the sensor is positioned at a fixed pre-defined axis while that under RF displays the score when the sensor is positioned arbitrarily, thus reflecting the influence to changes in axis orientation. The statistical measures of sensitivity and specificity display the true positive rate and the true negative rate of detecting HS and TO, respectively. The MAE, in sample units, gives the temporal accuracy of the algorithm for the correctly identified events. The KS test result is shown as a ratio of how many stride time data sets were not rejected by the null hypothesis compared to the total stride time data sets tested. The last row of the table shows the total number of GT gait events recorded from the test set data. The remaining rows present a comparison with the implemented methods in $\mathcal{A}_A$ and $\mathcal{A}_R$. Table III shows the mean and standard deviation of the performance scores for all indoor activities grouped together, only outdoor walking and all outdoor activities grouped together. The structure of Table III is similar to that of Table II, where each cell displays a score for detecting HS or TO from LF or

This article has been accepted for publication in a future issue of this journal, but has not been fully edited. Content may change prior to final publication. Citation information: DOI 10.1109/TNSRE.2016.2536278, IEEE Transactions on Neural Systems and Rehabilitation Engineering

TABLE III
MEAN (AND STANDARD DEVIATION) OF THE PERFORMANCE SCORES COMPUTED FOR ALL INDOOR ACTIVITIES GROUPED TOGETHER, ONLY OUTDOOR WALKING AND ALL OUTDOOR ACTIVITIES GROUPED TOGETHER. THE SCORES PRESENTED ARE COMPUTED FROM THE TEST DATA OF EACH ACTIVITY. $\mathcal{A}_{PM}$, $\mathcal{A}_A$ & $\mathcal{A}_R$ STAND FOR PROPOSED METHOD, METHOD [27] AND METHOD [4], RESPECTIVELY.

Performance measures		Indoor: Treadmill & Flat space				Outdoor							
		Walk & run				Walk				Walk & run			
		LF		RF		LF		RF		LF		RF	
		HS	TO	HS	TO	HS	TO	HS	TO	HS	TO	HS	TO
Sensitivity	$\mathcal{A}_{PM}$	**0.99** (0.00)	**0.97** (0.02)	**0.99** (0.00)	**0.99** (0.00)	**0.99** (0.00)	**0.98** (0.00)	**0.99** (0.00)	0.98 (0.01)	**0.99** (0.00)	**0.99** (0.00)	**0.99** (0.00)	**0.99** (0.00)
	$\mathcal{A}_A$	0.97 (0.05)	0.77 (0.16)	0.99 (0.01)	0.92 (0.10)	**0.99** (0.00)	0.94 (0.07)	0.45 (0.47)	**0.98** (0.00)	**0.99** (0.00)	0.89 (0.02)	0.70 (0.24)	0.54 (0.16)
	$\mathcal{A}_R$	0.84 (0.12)	0.75 (0.23)	0.82 (0.12)	0.71 (0.23)	0.98 (0.00)	0.97 (0.02)	**0.99** (0.00)	**0.98** (0.00)	0.70 (0.02)	0.43 (0.04)	0.69 (0.02)	0.44 (0.03)
Specificity	$\mathcal{A}_{PM}$	**0.99** (0.00)	**0.97** (0.03)	**0.99** (0.00)	**0.99** (0.00)	**0.99** (0.00)	**0.98** (0.01)	**0.99** (0.00)	0.98 (0.02)	**0.99** (0.00)	**0.99** (0.00)	**0.99** (0.00)	**0.99** (0.00)
	$\mathcal{A}_A$	0.92 (0.12)	0.08 (0.12)	0.84 (0.21)	0.06 (0.11)	0.83 (0.21)	0.01 (0.02)	0.63 (0.53)	0.04 (0.07)	0.84 (0.07)	0.19 (0.24)	0.72 (0.20)	0.01 (0.02)
	$\mathcal{A}_R$	0.95 (0.08)	0.85 (0.11)	0.94 (0.05)	0.82 (0.11)	**0.99** (0.00)	0.97 (0.02)	**0.99** (0.00)	**0.98** (0.00)	**0.99** (0.00)	0.71 (0.02)	0.96 (0.02)	0.71 (0.02)
MAE (in samples)	$\mathcal{A}_{PM}$	**0.92** (0.93)	1.50 (1.28)	**1.02** (0.99)	**1.17** (1.12)	**0.78** (0.77)	**0.80** (0.99)	**0.66** (0.79)	**0.93** (1.13)	1.29 (1.08)	1.82 (1.32)	**1.08** (0.91)	1.50 (1.23)
	$\mathcal{A}_A$	1.08 (1.06)	1.89 (1.52)	1.05 (0.97)	1.27 (1.21)	1.03 (0.88)	1.68 (1.68)	0.88 (0.93)	0.99 (1.12)	**1.13** (0.96)	2.50 (1.44)	1.64 (1.16)	1.51 (1.20)
	$\mathcal{A}_R$	1.04 (1.05)	**1.28** (1.17)	1.27 (1.22)	1.30 (1.24)	0.98 (0.95)	1.02 (1.00)	0.75 (0.82)	1.21 (1.18)	1.23 (1.05)	**1.23** (1.08)	1.30 (1.19)	**1.22** (1.22)
KS test ($\frac{\text{datasets not rejected}}{\text{total datasets tested}}$)	$\mathcal{A}_{PM}$	**12/12**	**12/12**	**12/12**	**12/12**	**3/3**	**3/3**	**3/3**	**3/3**	**3/3**	**3/3**	**3/3**	**3/3**
	$\mathcal{A}_A$	6/12	0/12	5/12	0/12	1/3	0/3	0/3	0/3	1/3	0/3	0/3	0/3
	$\mathcal{A}_R$	5/12	5/12	4/12	4/12	**3/3**	**3/3**	**3/3**	**3/3**	0/3	0/3	0/3	0/3
No. of GT gait events		6848	6837	6847	6842	566	562	565	562	1266	1264	1267	1264

RF, for a particular environment and activity (listed at the top of the table). The best performance scores have been shown as bolded font in both tables. Fig. 5 shows the mean F1 score of all algorithms for detecting HS and TO in indoor and outdoor environments, obtained using all subjects' data.

V. DISCUSSION AND CONCLUSION

The experiments were specifically designed to test the performance of the algorithm on various aspects of robustness in a real-world setting. The objective of conducting experiments on a treadmill, in an indoor space and on an outdoor street was to assess the performance in a variety of environmental conditions consisting of different surfaces, varying inclinations and regular turns. The aim of having fixed and arbitrary sensor orientations on the left and right ankles was to evaluate the influence of changes in axis orientation on the method's performance in these environments. Similarly, the goal of defining walking and running activities was to evaluate the performance at different gait speeds. Most gait event detection algorithms, such as $\mathcal{A}_A$ and $\mathcal{A}_R$, have been developed from walking data collected in indoor settings. The proposed algorithm demonstrates good performance for detecting both HS and TO from indoor walking data, implied by the high sensitivity, specificity and F1 scores shown in Table II and Fig. 5. Moreover, it detects them with high temporal accuracy shown by the low MAE values that are below one sample and the KS test results that do not reject any of the four data sets tested. In comparison, $\mathcal{A}_R$ also shows high performance scores for detecting both HS and TO, while $\mathcal{A}_A$ detects HS significantly better than TO ($p<0.05$). Although $\mathcal{A}_A$ has an average MAE of below one sample, the low KS test result indicates the occurrence of excessive false positives, especially for detecting TO. All algorithms exhibit no influence to changes in axis orientation with no significant difference between the F1 scores of the left and right foot ($p>0.05$). The proposed method also exhibits robustness to different gait speeds in indoor environments. It has high performance scores for all the indoor activities (walk and run) grouped together, as shown in Table III and Fig. 5. While $\mathcal{A}_R$ had exhibited good performance for indoor walking, it underperforms when running is included, with a significantly lower F1 score as compared to walking ($p<0.05$). Moreover, when running is included, $\mathcal{A}_R$'s performance decreases even more for detecting TO as compared to HS ($p<0.05$). In contrast to the controlled indoor experiments, the outdoor experiments were semi-controlled and representative of humans' natural environment in the real-world. The outdoor walking and running data grouped together plausibly represented the most diverse scenario, with unconstrained outdoor conditions and different gait speeds. The proposed method demonstrated good performance in this scenario, implied by the high performance scores shown in Table III and Fig. 5, with no significant difference between the indoor and outdoor F1 scores ($p>0.05$). It also performed well in terms of temporal accuracy, with an average MAE of 1.42 samples and none of the datasets being rejected by the KS test. Both $\mathcal{A}_A$ and $\mathcal{A}_R$ had their lowest

This article has been accepted for publication in a future issue of this journal, but has not been fully edited. Content may change prior to final publication. Citation information: DOI 10.1109/TNSRE.2016.2536278, IEEE Transactions on Neural Systems and Rehabilitation Engineering

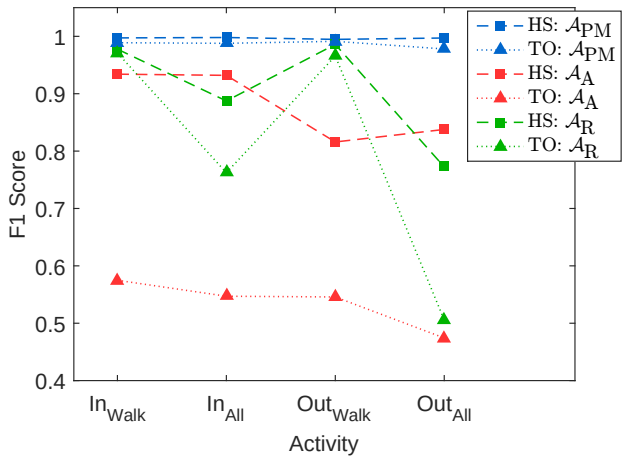

Fig. 5. Mean F1 scores of all algorithms for detecting HS and TO in indoor and outdoor environments. The mean values for each given activity on the x-axis were calculated by averaging the F1 score values obtained using data of all subjects. The activities labelled In_{Walk}, In_{All}, Out_{Walk} and Out_{All} represent only indoor (flat space) walking, all indoor activities grouped together, only outdoor walking and all outdoor activities grouped together, respectively. The mean F1 score of detecting HS for a particular activity is shown as a square while that for detecting TO is shown as a triangle. The F1 score reaches its best value at 1 and worst at 0. $\mathcal{A}_{PM}$, $\mathcal{A}_{A}$ & $\mathcal{A}_{R}$ stand for Proposed Method, method [27] and method [4], respectively.

F1 scores for detecting events in this scenario as compared to all other environments in which they were tested. It was also significantly lower than their F1 scores for indoor activities grouped together (p<0.05). This might be attributed to the fact that both $\mathcal{A}_{A}$ and $\mathcal{A}_{R}$ were designed using indoor walking data only and since activities in outdoor conditions are more uncontrolled and dynamic, they introduce more noise in the accelerometer signals. Moreover, it is difficult to make an objective comparison between algorithms that were designed using different datasets and protocols. However, the results exhibit that the proposed method could be directly applied in different environments for long-term applications.

The ability of the proposed method to effectively tackle real-world challenges is enabled by the use of domain knowledge to guide the time-frequency analysis. Knowledge about the event-cycle frequency relationship present in gait is utilized to logically reason around choosing the appropriate mother wavelet (Morlet), in order to gain a distinct separation between the event and cycle frequencies in time, as shown in Fig. 1b and 1c. It is also utilized in the tracking procedure to tackle any gait speed speed changes, which is a substantial requirement for many real-world applications. In addition, the scale-frequency relationship of the Morlet is used to select the appropriate scales for analysis based on the frequency of the activity. While the proposed method was developed with the accelerometer placed around the ankle, it still remains to be investigated if and how the technique may be utilized to detect events from other parts of the body. With an arbitrary sensor placement on the body, it might be challenging to attribute the sensor information to the left or right foot, thus making it difficult to identify and label individual events. However, it would be possible to detect gait cycles using the tracking procedure presented in this method. Another limitation of the proposed method is that it has been validated only on healthy gait. Future work is needed to test the method on pathological gait and make any required adaptations to the algorithm. A service has been provided (http://islab.hh.se/mediawiki/Gait_events) to assist interested readers in making use of the proposed method with their data.

To conclude, this paper proposes a novel approach that exhibits how domain knowledge about human gait can be incorporated into time-frequency analysis in order to develop a robust algorithm that can detect gait events from long-term accelerometer signals. The ability of the algorithm to effectively adapt in real-world scenarios is validated by experiments done in indoor and outdoor environments that involve different gait speeds, changing walking terrains, varying surface inclinations and regular turns among other things. The proposed algorithm is shown be accurate and robust with consistently high performance scores across all datasets.

APPENDIX

This section elaborates on the details required to implement the tracking procedure to tackle changes in gait speeds. As explained earlier in Section II-B2, in order to track the transitions of the event and cycle coefficients, an overlapping running window is taken along the temporal axis of the CWT coefficients. In principle, a window size that captures the information about one gait cycle would be sufficient but it is practically desired to be large enough to account for signal noise and should thus include additional gait cycles. In this paper, the running window size is taken to be 3 or 6 seconds with a 50% overlap. The entire tracking procedure within a given window consists of the following steps (refer Fig. 6):

i. The energy density spectrum $E_{s,r}$ of the CWT coefficients selected from the current window is computed using eq. 3 as $E_{s,r} = \sum_{n=rM}^{(r+1)M-1} |W_n(s)|^2$ where $s \in [1, s_{\max}]$, r is the window index and M is the window hop size, i.e. the number of samples by which each successive window is advanced in time. $E_{s,r}$ highlights the dominant energetic scales of event and cycle in the current window r.

ii. The *a priori* estimate $E^{-}_{s,r}$ is cross-correlated ($\star$) with $E_{s,r}$ in order to measure the scale delay τ_r between them, calculated as $\tau_r = \arg\max_{s\in[1,s_{\max}]}(E^{-}_{s,r} \star E_{s,r})$. For the first window ($r$=1), the *a priori* estimate formulated in eq. 6 is used. Scale delay τ_r reflects the change in gait speed from the previous window. However, very fast transitions in gait speeds would cause large shifts in the local signal energy. As such, the Gaussian mixture parameters in $E^{-}_{s,r}$ may be very different from that of $E_{s,r}$, resulting in an incorrect τ_r value due to poor alignment of the two signals. Thus, Constraint I is used to verify that τ_r lies within the expected scale bounds:

$$\text{Constraint I}: \begin{cases} \mu^{-}_{e,r} + \tau_r > 1 \\ \mu^{-}_{c,r} + \tau_r < s_{\max} \end{cases} \tag{11}$$

iii. If Constraint I is satisfied, then the *a priori* estimate $E^{-}_{s,r}$ is updated to form an *a posteriori* estimate $\hat{E}_{s,r}$. This is done by first calculating a scale, $s_{\lambda,r} = \arg\min E_{s,r}$ where $s \in [\mu^{-}_{e,r} + \tau_r,\ \mu^{-}_{c,r} + \tau_r]$, that helps to distinguish

This article has been accepted for publication in a future issue of this journal, but has not been fully edited. Content may change prior to final publication. Citation information: DOI 10.1109/TNSRE.2016.2536278, IEEE Transactions on Neural Systems and Rehabilitation Engineering

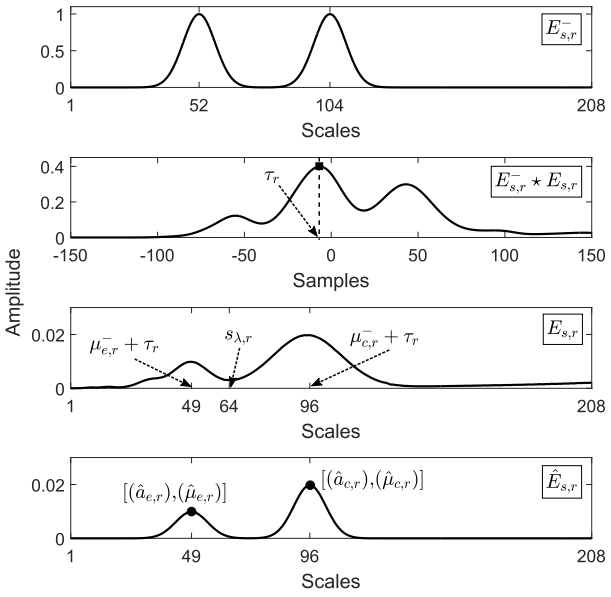

Fig. 6. Example of the steps involved in the tracking procedure of window index r=1. The first subfigure shows the *a priori* energy density spectrum estimate E_s^-, to start the tracking procedure. The second subfigure shows the scale delay, τ_r in the cross-correlation result of $(E^-_{s,r} \star E_{s,r})$. The third subfigure shows $s_{\lambda,r}$ which distinguishes the scales corresponding to event and cycle energies in $E_{s,r}$. The fourth subfigure shows the *a posteriori* estimate $\hat{E}_s$ whose parameters are stored after both constraints are satisfied.

the range of scales in which the event and cycle energies lie in $E_{s,r}$. The set of equations used to form the *a posteriori* estimate $\hat{E}_{s,r}$ are:

$$\begin{aligned}
\hat{\mu}_{e,r} &= \arg\max_{s\in[1,s_{\lambda,r}]} E_{s,r} \\
\hat{a}_{e,r} &= \max_{s\in[1,s_{\lambda,r}]} E_{s,r} \\
\hat{\sigma}_{e,r} &= \sigma^-_{e,r} \\
\hat{\mu}_{c,r} &= \arg\max_{s\in[s_{\lambda,r},s_{\max}]} E_{s,r} \\
\hat{a}_{c,r} &= \max_{s\in[s_{\lambda,r},s_{\max}]} E_{s,r} \\
\hat{\sigma}_{c,r} &= \sigma^-_{c,r}
\end{aligned} \tag{12}$$

To verify that the updated Gaussian means in $\hat{E}_{s,r}$ uphold the frequency relationship stated in eq. 5, a constraint is applied as Constraint II:$1.9 \leq \frac{\hat{\mu}_{c,r}}{\hat{\mu}_{e,r}} \leq 2.1$. The relationship is relaxed by 5% to accommodate effects of signal noise and low frequency resolution in finer scales [44].

iv. If either of the constraints are not satisfied, then curve fitting of a two term 1-D Gaussian mixture is performed over $E_{s,r}$ and the resulting fit parameters are used to constitute $\hat{E}_{s,r}$. Since curve fitting is sensitive to starting point declarations, the event-cycle frequency relationship can be utilized to define two sets of possible starting points for $\{a_e, \mu_e, \sigma_e, a_c, \mu_c, \sigma_c\}$, to guide the fitting procedure in order to obtain a good fit. These are $Set1 = \{a_\chi, \mu_\chi/2, s_{\max}/16, a_\chi, \mu_\chi, s_{\max}/8\}$ and $Set2 = \{a_\chi, \mu_\chi, s_{\max}/16, a_\chi, 2\mu_\chi, s_{\max}/8\}$ where μ_χ is the most energetic scale in $E_{s,r}$ i.e. $\arg\max_{s\in[1,s_{\max}]} E_{s,r}$ and a_χ is the corresponding energy value at that scale i.e. $\max_{s\in[1,s_{\max}]} E_{s,r}$. Thus, two fits over $E_{s,r}$ are obtained by using each set as the starting point. In order to decide the better fit, an initial check is made to verify whether the fit parameters lie within the expected bounds, i.e. $\{a_e, a_c\} > 0$ and $\{\mu_e, \mu_c, \sigma_e, \sigma_c\} \in [1, s_{\max}]$, and a fit that lies outside these bounds is rejected. If both fits lie within the expected bounds, then root mean square error (RMSE) is computed for both the fits. In the RMSE computation, only high energy density values are taken into account, and the lower 10% of $E_{s,r}$ is excluded to remove its influence on the RMSE calculation as it does not contribute to the event and cycle energies, as shown in Fig. 7. The better fit is chosen as the one with the lowest RMSE value, following which Constraint II is verified again to ensure that the fit is correct. In case of violation, the *a posteriori* estimate $\hat{E}_{s,r}$ is constituted directly from the existing parameters of the *a priori* estimate $E^-_{s,r}$ without any update from the current window, i.e. $\hat{E}_{s,r} \leftarrow E^-_{s,r}$.

v. The Gaussian parameters in *a posteriori* estimate $\hat{E}_{s,r}$ and scale $s_{\lambda,r}$ computed in the current window are stored following which $\hat{E}_{s,r}$ serves as the prior for the next window, i.e. $E^-_{s,r+1} \leftarrow \hat{E}_{s,r}$.

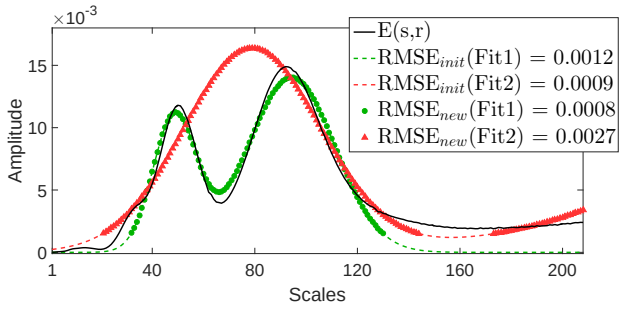

Fig. 7. Example of how RMSE computation is influenced by the lower energy values in $E_{s,r}$. Even though Fit1 is a better fit than Fit2, initially it gives a higher RMSE$_{init}$ because it includes lower energy scales corresponding to the lower 10% values of $E_{s,r}$. However, if these lower energy scales are excluded, then Fit1 gives a lower RMSE$_{new}$, indicating that it is a better fit as compared to Fit2.

ACKNOWLEDGMENT

The authors would like to thank Thomas Lithén for preparing the experimental setup. They would also like to thank Prof. Josef Bigun for his valuable insights on wavelet transforms and Prof. Eric Järpe for discussions on statistical inference.

REFERENCES

[1] A. H. Snijders, B. P. van de Warrenburg, N. Giladi, and B. R. Bloem, "Neurological gait disorders in elderly people: clinical approach and classification," *The Lancet Neurology*, vol. 6, no. 1, pp. 63–74, 2007.

[2] R. Williamson and B. Andrews, "Gait event detection for FES using accelerometers and supervised machine learning," *Rehab. Eng., IEEE Trans. on*, vol. 8, no. 3, pp. 312–319, 2000.

[3] A. Mansfield and G. M. Lyons, "The use of accelerometry to detect heel contact events for use as a sensor in FES assisted walking," *Med. Eng. & Phys.*, vol. 25, no. 10, pp. 879–885, 2003.

[4] J. Rueterbories, E. G. Spaich, and O. K. Andersen, "Gait event detection for use in FES rehabilitation by radial and tangential foot accelerations," *Med. Eng. & Phys.*, vol. 36, no. 4, pp. 502–508, 2014.

[5] T. A. Wren, G. E. G. III, S. Õunpuu, and C. A. Tucker, "Efficacy of clinical gait analysis: A systematic review," *Gait Posture*, vol. 34, no. 2, pp. 149–153, 2011.

[6] M. J. Socie, R. W. Motl, J. H. Pula, B. M. Sandroff, and J. J. Sosnoff, "Gait variability and disability in multiple sclerosis," *Gait Posture*, vol. 38, no. 1, pp. 51–55, 2013.

[7] V. Dietz, "Neurophysiology of gait disorders: present and future applications," *Electroencephalography and Clinical Neurophysiology*, vol. 103, no. 3, pp. 333–355, 1997.

[8] M. Woollacott and A. Shumway-Cook, "Attention and the control of posture and gait: a review of an emerging area of research," *Gait Posture*, vol. 16, no. 1, pp. 1–14, 2002.

[9] T. IJmker and C. Lamoth, "Gait and cognition: The relationship between gait stability and variability with executive function in persons with and without dementia," *Gait Posture*, vol. 35, no. 1, pp. 126–130, 2012.

[10] P. B. Shull, W. Jirattigalachote, M. A. Hunt, M. R. Cutkosky, and S. L. Delp, "Quantified self and human movement: A review on the clinical impact of wearable sensing and feedback for gait analysis and intervention," *Gait Posture*, vol. 40, no. 1, pp. 11–19, 2014.

[11] D. A. Bruening and S. T. Ridge, "Automated event detection algorithms in pathological gait," *Gait Posture*, vol. 39, no. 1, pp. 472–477, 2014.

[12] K. Aminian, B. Najafi, and C. B "Spatio-temporal parameters of gait measured by an ambulatory system using miniature gyroscopes," *J. of Biomechanics*, vol. 35, no. 5, pp. 689–699, 2002.

[13] J. M. Jasiewicz, J. H. Allum, J. W. Middleton, A. Barriskill, P. Condie, B. Purcell, and R. C. T. Li, "Gait event detection using linear accelerometers or angular velocity transducers in able-bodied and spinal-cord injured individuals," *Gait Posture*, vol. 24, no. 4, pp. 502–509, 2006.

[14] P. Lopez-Meyer, G. Fulk, and E. Sazonov, "Automatic detection of temporal gait parameters in poststroke individuals," *Info. Tech. in Biomed., IEEE Trans. on*, vol. 15, no. 4, pp. 594–601, 2011.

[15] T. Everett and C. Kell, *Human movement: an introductory text*. Elsevier health sciences, 2010.

[16] J. R. Rebula, L. V. Ojeda, P. G. Adamczyk, and A. D. Kuo, "Measurement of foot placement and its variability with inertial sensors," *Gait Posture*, vol. 38, no. 4, pp. 974 – 980, 2013.

[17] J. Rueterbories, E. G. Spaich, B. Larsen, and O. K. Andersen, "Methods for gait event detection and analysis in ambulatory systems," *Med. Eng. & Phys.*, vol. 32, no. 6, pp. 545–552, 2010.

[18] B. Greene, D. McGrath, R. ONeill, K. ODonovan, A. Burns, and B. Caulfield, "An adaptive gyroscope-based algorithm for temporal gait analysis," *Med. Bio. Eng. Comp.*, vol. 48, no. 12, 2010.

[19] A. Salarian, H. Russmann, F. Vingerhoets, C. Dehollaini, Y. Blanc, P. Burkhard, and K. Aminian, "Gait assessment in parkinson's disease: toward an ambulatory system for long-term monitoring," *Biomed. Eng., IEEE Trans. on*, vol. 51, no. 8, pp. 1434–1443, 2004.

[20] I. Pappas, M. Popovic, T. Keller, V. Dietz, and M. Morari, "A reliable gait phase detection system," *Neural Sys. and Rehab. Eng., IEEE Trans. on*, vol. 9, no. 2, pp. 113–125, 2001.

[21] A. Mannini, V. Genovese, and A. Sabatin, "Online decoding of hidden markov models for gait event detection using foot-mounted gyroscopes," *Biomed. and Health Info., IEEE J. of*, vol. 18, no. 4, pp. 1122–1130, 2014.

[22] J. Lee and E. Park, "Quasi real-time gait event detection using shank-attached gyroscopes," *Med. & Bio. Eng. & Comp.*, vol. 49, no. 6, pp. 707–712, 2011.

[23] J. J. Kavanagh and H. B. Menz, "Accelerometry: A technique for quantifying movement patterns during walking," *Gait Posture*, vol. 28, no. 1, pp. 1–15, 2008.

[24] R. Selles, M. Formanoy, J. Bussmann, P. Janssens, and H. Stam, "Automated estimation of initial and terminal contact timing using accelerometers; development and validation in transtibial amputees and controls," *Neural Sys. and Rehab. Eng., IEEE Trans. on*, vol. 13, no. 1, pp. 81–88, 2005.

[25] R. Torrealba, J. Cappelletto, L. Fermn-Leon, J. Grieco, and G. Fernández-López, "Statistics-based technique for automated detection of gait events from accelerometer signals," *Electronics Letters*, vol. 46, no. 22, pp. 1483–1485, 2010.

[26] A. Sant'Anna and N. Wickström, "A symbol-based approach to gait analysis from acceleration signals: Identification and detection of gait events and a new measure of gait symmetry," *Info. Tech. in Biomed., IEEE Trans. on*, vol. 14, no. 5, pp. 1180–1187, 2010.

[27] M. Aung, S. Thies, L. Kenney, D. Howard, R. Selles, A. Findlow, and J. Goulermas, "Automated detection of instantaneous gait events using time frequency analysis and manifold embedding," *Neural Sys. and Rehab. Eng., IEEE Trans. on*, vol. 21, no. 6, pp. 908–916, 2013.

[28] M. Yoneyama, Y. Kurihara, K. Watanabe, and H. Mitoma, "Accelerometry-based gait analysis and its application to parkinson's disease assessment - part 1: Detection of stride event," *Neural Sys. and Rehab. Eng., IEEE Trans. on*, vol. 22, no. 3, pp. 613–622, 2014.

[29] H.-K. Lee, J. You, S.-P. Cho, S.-J. Hwang, D.-R. Lee, Y.-H. Kim, and K.-J. Lee, "Computational methods to detect step events for normal and pathological gait evaluation using accelerometer," *Electronics Letters*, vol. 46, no. 17, pp. 1185–1187, 2010.

[30] D. Lai, R. Begg, and M. Palaniswami, "Computational intelligence in gait research: A perspective on current app. and future challenges," *Info. Tech. in Biomed., IEEE Trans. on*, vol. 13, no. 5, pp. 687–702, 2009.

[31] T. Chau, "A review of analytical techniques for gait data. part 2: neural network and wavelet methods," *Gait Posture*, vol. 13, no. 2, pp. 102–120, 2001.

[32] D. Gouwanda and S. Senanayake, "Application of hybrid multi-resolution wavelet decomposition method in detecting human walking gait events," in *Soft Comp. and Pattern Recog., Int. Conf. of*, 2009, pp. 580–585.

[33] P. Forsman, E. Toppila, and E. Haeggstrom, "Wavelet analysis to detect gait events," in *Eng. in Med. and Bio. Society, Annual Int. Conf. of the IEEE*, 2009, pp. 424–427.

[34] J. McCamley, M. Donati, E. Grimpampi, and C. Mazzà, "An enhanced estimate of initial contact and final contact instants of time using lower trunk inertial sensor data," *Gait Posture*, vol. 36, no. 2, pp. 316–318, 2012.

[35] M. Yuwono, S. W. Su, Y. Guo, B. D. Moulton, and H. T. Nguyen, "Unsupervised nonparametric method for gait analysis using a waist-worn inertial sensor," *App. Soft Comp.*, vol. 14, Part A, pp. 72–80, 2014.

[36] D. Novak, P. Reberek, S. M. M. D. Rossi, M. Donati, J. Podobnik, T. Beravs, T. Lenzi, N. Vitiello, M. C. Carrozza, and M. Munih, "Automated detection of gait initiation and termination using wearable sensors," *Med. Eng. & Phys.*, vol. 35, no. 12, pp. 1713–1720, 2013.

[37] P. Addison, J. Walker, and R. Guido, "Time-frequency analysis of biosignals," *Eng. in Med. and Biology Magazine, IEEE*, vol. 28, no. 5, pp. 14–29, 2009.

[38] J. Rafiee, M. Rafiee, N. Prause, and M. Schoen, "Wavelet basis functions in biomedical signal processing," *Expert Sys. with App.*, vol. 38, no. 5, pp. 6190–6201, 2011.

[39] J. Lilly and S. Olhede, "Higher-order properties of analytic wavelets," *Signal Proc., IEEE Trans. on*, vol. 57, no. 1, pp. 146–160, 2009.

[40] C. Torrence and G. P. Compo, "A practical guide to wavelet analysis," *Bulletin of the American Meteo. Soc.*, vol. 79, no. 1, pp. 61–78, 1998.

[41] M. Hanlon and R. Anderson, "Real-time gait event detection using wearable sensors," *Gait Posture*, vol. 30, no. 4, pp. 523–527, 2009.

[42] T. Fawcett, "An introduction to ROC analysis," *Pattern Recognition Letters*, vol. 27, no. 8, pp. 861–874, 2006.

[43] J. Massey, Frank J., "The kolmogorov-smirnov test for goodness of fit," *J. of the American Stat. Assoc.*, vol. 46, no. 253, pp. 68–78, 1951.

[44] B. K. Alsberg, A. M. Woodward, and D. B. Kell, "An introduction to wavelet transforms for chemometricians: A time-frequency approach," *Chemometrics and Intellig. Lab. Sys.*, vol. 37, no. 2, pp. 215–239, 1997.

Siddhartha Khandelwal received his Master degree in Robotics from WUT, Warsaw, Poland, and ECN, Nantes, France. He is currently a PhD student at the School of Information Technology, Halmstad University, Sweden. His current research interests are in wearable sensors and biomedical signal processing.

Nicholas Wickström received his Ph.D. degree in computer engineering from Chalmers University of Technology, Gothenburg, Sweden, in 2004. He is currently an Associate Professor at the School of Information Technology, Halmstad University, Sweden. His current research interests include biomedical sensing and signal processing.
Dr. Wickström is a member of IEEE.